European Journal of Medicinal Chemistry 45 (2010) 4570–4577

Contents lists available at ScienceDirect

European Journal of Medicinal Chemistry

journal homepage: http://www.elsevier.com/locate/ejmech

Original article

An alignment independent 3D QSAR study of the antiproliferative activity of 1,2,4,5-tetraoxanes

Ilija N. Cvijetić [a], Željko P. Žižak [b], Tatjana P. Stanojković [b], Zorica D. Juranić [b], Nataša Terzić [c], Igor M. Opsenica [a], Dejan M. Opsenica [c], Ivan O. Juranić [a], Branko J. Drakulić [c,*]

[a] Faculty of Chemistry, University of Belgrade, Studentski Trg 12-16, 11000 Belgrade, Serbia
[b] Institute for Oncology and Radiology of Serbia, Pasterova 14, 11000 Belgrade, Serbia
[c] Institute for Chemistry, Technology and Metallurgy, Njegoševa 12, 11000 Belgrade, Serbia

ARTICLE INFO

Article history:
Received 18 December 2009
Received in revised form
11 July 2010
Accepted 12 July 2010
Available online 11 August 2010

Keywords:
Tetraoxanes
3D QSAR
GRIND
Antiproliferative activity
Multiple linear regression

ABSTRACT

An alignment-free 3D QSAR study on antiproliferative activity of the thirty-three 1,2,4,5-tetraoxane derivatives toward two human dedifferentiated cell lines was reported. GRIND methodology, where descriptors are derived from GRID molecular interaction fields (MIF), were used. It was found that pharmacophoric pattern attributed to the most potent derivatives include amido NH of the primary or secondary amide, and the acetoxy fragments at positions 7 and 12 of steroid core which are, along with the tetraoxane ring, common for all studied compounds. Independently, simple multiple regression model obtained by using the whole-molecular properties, confirmed that the hydrophobicity and the H-bond donor properties are the main parameters influencing potency of compounds toward human cervix carcinoma (HeLa) and human malignant melanoma (FemX) cell lines. Corollary, similar structural motifs are found to be important for the potency toward both examined cell lines.

1. Introduction

The discovery that artemisinin, an active principle of *Artemisia annua* L., expresses a significant antimalarial activity, especially against chloroquine resistant (CQR) strains [1], opened a new approaches for combating malaria. Since early 1980s hundreds of semisynthetic and synthetic peroxides were developed and tested as antimalarials [2]. Discovering a pronounced antimalarial activity of inexpensive 1,2,4,5-tetraoxanes against CQR *Plasmodium falciparum* strains, opened new opportunities in combating this pestilence [3]. Significant efforts have been made to find improved procedures for designing and synthesizing new derivatives with higher potency [4,5]; as were reviewed [2,6].

Tetraoxanes obtained from cholic acid and derivatives are of particular interest because of their amphiphilic structure, which facilitate passage through various cell membranes [7,8]. New class of mixed steroidal tetraoxanes[1] obtained from cholic [9–11] and deoxycholic [12] acids are much more potent as antimalarials both *in vitro* and *in vivo*, in respect to bis-steroidal analogues. Along with steroid-based, the tetraoxanes derived from cyclohexane were also tested as antimalarials and showed significant *in vitro* and *in vivo* potencies [11,13]. Many tetraoxane derivatives also exhibited antiproliferative activity against various human cancer cell lines, with morphological appearance reminiscent for apoptosis [7,14], and showed very low cytotoxicity toward healthy human cells. In references given in Table 1, antimalarial activity of **1**–**33** was also described. It should be noted that antiproliferative and antimalarial potencies of studied compounds are poorly intercorrelated (Supplementary material, Table S1).

2. Results and discussion

Synthesis, antimalarial and antiproliferative activity of compounds **1**–**33** were reported previously. Detail description of all experimental procedures can be found in the following references (see also Table 1): For the compounds **1**–**5**, references [11,13]; for

Abbreviations: 3D QSAR, three-dimensional structure activity relationship; GRIND, grid independent descriptors; MIF, molecular interaction fields; IE, interaction energies; PCA, principal component analysis; PLS, partial least square; FFD, fractional factorial design; LV, latent variables; MLR, multiple linear regression; HeLa, human cervix carcinoma cells; FemX, human melanoma cells.

* Corresponding author. Tel.: +381 11 3336 738; fax: +381 11 2636 061.
E-mail address: bdrakuli@chem.bg.ac.rs (B.J. Drakulić).

[1] Term "mixed tetraoxanes" describes differently substituted 1,2,4,5-tetraoxacyclohexanes at positions 3 and 6, see reference [9].

0223-5234/$ – see front matter © 2010 Elsevier Masson SAS. All rights reserved.
doi:10.1016/j.ejmech.2010.07.019

Table 1
Structures and potencies toward HeLa and FemX cell lines of compounds **1**–**33**.

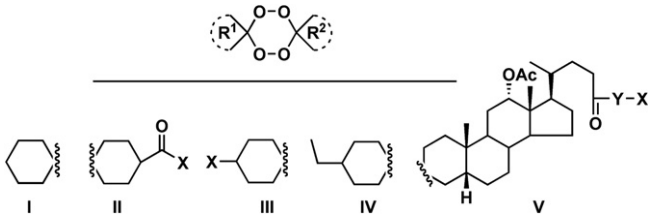

Compound no.	R^1	R^2	Y	X	$p(IC_{50})$ (HeLa)	$p(IC_{50})$ (FemX)	Ref.
1	I	II	/	$-OCH_3$	4.12	4.14	[11,13]
2	I	II	/	$-OH$	3.92	3.81	[11,13]
3	I	II	/	NH_2	3.94	3.92	[11,13]
4	I	II	/	$NHCH_2CH_2CH_3$	3.93	3.99	[11,13]
5	I	II	/	$NHCH_2CH_2N(CH_3)_2$	3.87	3.92	[11,13]
6	I	V	/	$-OCH_3$	4.74	5.20	[12]
7	I	V	/	$-OH$	5.16	4.60	[12]
8	I	V	–NH–	–H	5.28	5.22	[12]
9	I	V	–NH–	$-CH_2CH_2CH_3$	5.19	4.88	[12]
10	I	V	–N<	$-(CH_2CH_2CH_3)_2$	4.55	4.41	[12]
11	I	V	/		5.14	5.04	[12]
12	III	V	–OMe	–H	4.73	4.28	[9]
13	III	V	–OMe	$-CH_3$ (4″*R*)	4.96	4.13	[9]
14	III	V	–OMe	$-CH_3$ (4″*S*)	5.3	4.60	[9]
15	III	V	–OMe	–spiro-cyclopentyl	4.97	4.37	[9]
16	III	V	–OMe	–spiro-cyclooctyl	4.99	4.29	[9]
17[a]	V	V	–N<	$-(CH_2CH_2CH_3)_2$	3.98	4.32	[7,8]
18	V	V	/		4.05	4.1	[7,8]
19	V	V	/	–H	5.43	5.51	[7,8]
20	V	V	–NH–	$-CH_2CH_2CH_3$	4.48	4.64	[7,8]
21	V	V	/	$-OH$	5.28	5.38	[7,8]
22[a]	V	V	–NH–	$-CH_2C(O)OCH_3$	5.44	5.33	[7,8]
23	V	V	/		3.92	3.99	[7,8]
24	V	V	–NH–	–H	5.22	5.21	[7,8]
25	V	V	–NH–	$-CH_2CH_2CH_3$	5.08	4.59	[7,8]
26	V	V	/	$-OH$	5.04	5.12	[7,8]
27	V	V	/	$-OCH_3$	4.69	4.71	[7,8]
28	IV	V	–NH–	–H (4″*R*)	5.28	5.30	[9]
29	IV	V	–NH–	–H (4″*S*)	5.39	5.37	[9]
30	IV	V	–NH–	$-CH_3$ (4″*R*)	5.31	5.16	[9]
31	IV	V	–NH–	$-CH_3$ (4″*S*)	5.17	5.35	[9]
32	IV	V	–NH–	$-CH_2CH_3$ (4″*R*)	5.16	5.17	[9]
33	IV	V	–NH–	$-CH_2CH_3$ (4″*S*)	5.16	5.05	[9]

[a] For **17**–**21** R^1 and R^2 are *trans* to each other; for **22**–**27** R^1 and R^2 are *cis* to each other.

the compounds **6**–**11** [12]; **12**–**16** [9]; **19**, **20**, **21**, **24**–**27** [7]; **17**, **18**, **22**, **23**, also **19** and **24** [8]; and for the compounds **28**–**33** reference [9]. Description of computational procedures and GRIND [15,16] methodology are given in Supplementary material.

Potencies of both epimers (for **28**–**29**, **30**–**31**, **32**–**33**) were experimentally determined (Table 1), but the absolute configurations could not be assigned with confidence so far. Stereochemistry of epimers, given in Table 1, was assigned by analogy with the 4″-methyl analogues for which configuration at the stereogenic carbon have been unambiguously assigned by the X-ray analysis [8]. As the both epimers within each pair exert similar potency,[2] our models were unable to explain such small variation of potencies. Therefore we obtained two models. In the each model, one set of potency values were assigned to the one of the epimers (4*R*″ or 4*S*″) from the respective epimer pairs, to see whether one combination shows better predictivity and interpretability than the other; but models obtained were almost equal. The slight differences of TIP–TIP, DRY–DRY, and DRY–TIP correlograms (Supplementary material, Fig. S1) reflect different spatial position between 4″-ethyl group and the rest of steroid core. These differences did not have significant impact on final results.

2.1. HeLa model

Antiproliferative potencies of **1**–**33** ($p(IC_{50})$ values), have been used as a dependent variable. Initial models, for the both HeLa and

[2] The difference in potencies of each epimer pair is almost within experimental error, Table S2 in Supplementary material.

Table 2
Statistics of PLS model for antiproliferative potencies of **1**–**33** toward HeLa cells.

LVs	X variable explanation	X accumulation	SDEC	SDEP	r^2	q^2 (LOO)	q^2 (LTO)	q^2 (RG)
1	30.23	30.23	0.35	0.43	0.58	0.36	0.37	0.40
2	24.52	54.75	0.21	0.28	0.85	0.73	0.74	0.75
3	16.28	71.03	0.13	0.19	0.94	0.87	0.87	0.85

Abbreviations: SDEC – Standard Deviation of Error of Calculation, SDEP – Standard Deviation of Error of Prediction. One run of FFD variable selection using the following settings: 4 random groups; 20 SDEP; 20% dummies; and Comb/Var ratio = 2. Validation methods used for calculation of q^2 are: random groups (RG), leave two out (LTO), and leave one out (LOO).

FemX cells, identified compound **11** as an outlier, having the significantly higher experimentally obtained potency than predicted. Since there was no structural indication for such behaviour, we could not offer any valid explanation.

Initial PLS model was built by using five latent variables (LVs). After one cycle of FFD, number of variables was reduced from 1190 to 761 for the final model. Model had improved statistical quality, while PLS coefficients plot appear almost unchanged in respect to initial model. The optimal number of PLS components (LVs) was chosen by monitoring the changes in the model's predictivity index (q^2), evaluated by applying the cross-validation procedure available in Pentacle. For the interpretation 3LV were used.

The dependence of y_{calc} *vs.* y_{exp} is shown on Fig. S2 in Supplementary material. Statistical data for this model are shown in Table 2.

Fig. 1 shows 3LV PLS coefficients plot for the HeLa model. Among the auto-correlograms, the N1–N1 and the TIP–TIP comprise several variables having high intensity, and consequently have significant impact on the model. The vast majority of positively correlated bars are located on the left side of each of the correlograms (representing smaller node–node distances), and most of the negatively correlated variables are positioned on larger node–node distances, *i.e.* on the right side of correlograms. This shows that the structural elements which exert positive impact on potency, as described by each correlogram, are located closer to each other in molecules than those ones having negative impact. Among the cross-correlograms, the most important ones are O–N1 and N1–TIP. Association of structural elements of studied molecules with variables having the highest impact on model is exemplified in Fig. 2. Brief description of variables having high impact on model is given in Table 3.

Summarizing, structural elements positively correlated with the potency toward the HeLa cells are:

- Acetoxy groups (HBA) associated with N1 probe area (with IEs from −6.35 to −5.65 kcal/mol), and the distal alkyl area (17.28–17.60 Å) associated with the TIP probe (as expressed by variable 1125), Fig. 2c.
- Acetoxy group associated with N1 probe area having the same IEs as above, on distance of 7.04–7.36 Å to various HBA regions (complementary to N1 probe), as shown by variable 260.
- Unhindered HBD region around primary or secondary amide NH (associated with the O probe with IEs from −5.6 to

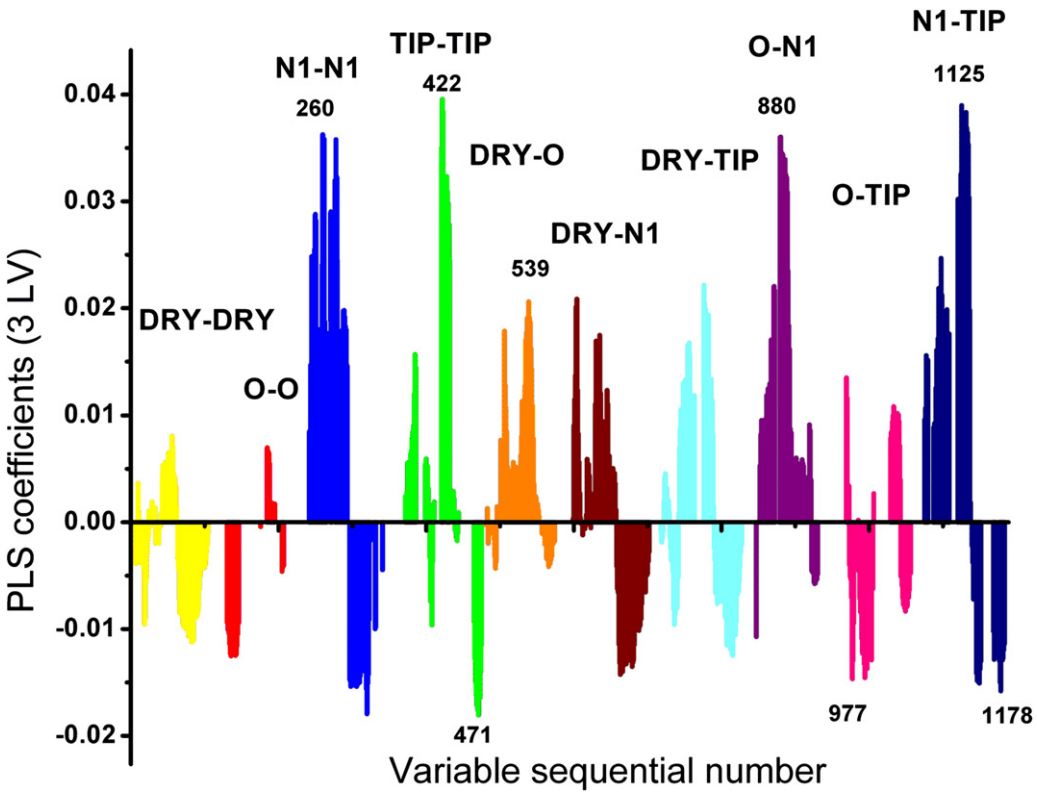

Fig. 1. 3LV PLS coefficients plot for the model on antiproliferative potencies of **1**–**33** toward HeLa cells. Graph shows all auto- and cross-correlograms. The most intensive variables are labeled by sequential numbers.

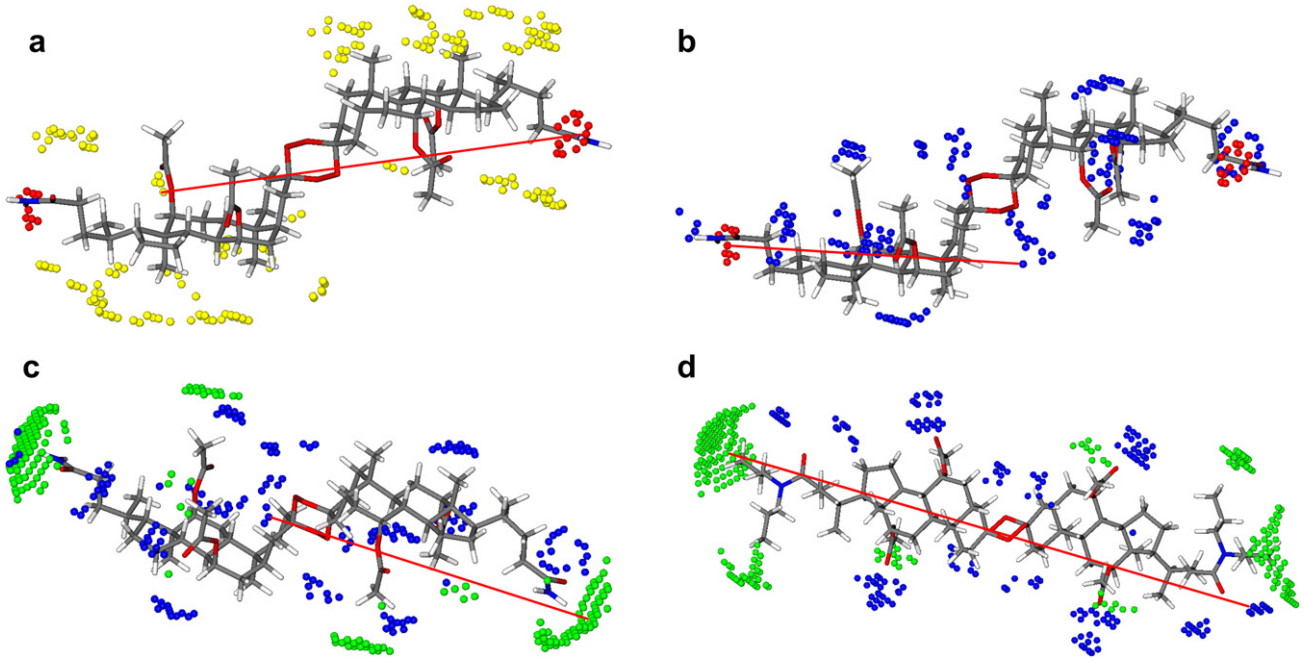

Fig. 2. Association of structural fragments with variables: (a) 539 (DRY–O); (b) 880 (O–N1); (c) 1125 (N1–TIP), for compound **19**; and (d) 1178 (N1–TIP), for compound **17**.

−4.7 kcal/mol) and the distal hydrocarbon area on distance of 20.16–20.48 Å, as shown by variable 539, Fig. 2a.

– The amido HBDs of the primary or the secondary NH groups connected to C24 atom of the cholic acid core, and HBAs of the acetoxy group or of the tetraoxane ring, on the spatial distances between 15.04 and 15.36 Å, as expressed by variable 880, Fig. 2b.

The most potent compounds among **1**–**33** posses HBDs as the primary (**8**, **19**, **24**, **28**, **29**) or secondary amide (**9**, **20**, **22**, **25**, **30**–**33**) hydrogen, or as carboxylic group (**7**, **21**, **26**), all described by variables having the highest impact on model.

The less potent compounds exert weaker interactions with HBA probe, compared to the more potent analogues, probably because of steric hindrance of the HBDs. The most favourable IEs of the O probe are in range of −5.6 to −4.7 kcal/mol, for compounds **7**–**9**, **19**–**22**, **24**–**26**, and **28**–**33**. Bulky alkyl groups in proximity to the amido nitrogen attenuate potency of compounds. Compounds having tertiary amido moiety, and consequently incapable to act as HBDs, are the least potent ones. On the basis of the observations derived from the model, likely that HBDs of the terminal area of molecules are important for potency.

2.2. FemX model

Antiproliferative potency data of **1**–**33** toward FemX cells are used as a dependent variable in this model. In the initial model compounds **6** and **11** were detected as outliers, having experimentally obtained potencies higher than predicted. Statistical parameters are given in Table 4. The same methods as in the HeLa model are applied for the variable selection, and the cross-validation (1 cycle of FFD reduces the number of variables from 1190 to 775).

In the Table 5, important variables for the model are shown, and their association with the structural fragments of molecules. Graph of y_{calc} *vs*. y_{exp} is given in Supplementary material, Fig. S3.

Fig. 3 shows 3LV PLS coefficient plot. The pattern of variables on this plot is very similar to the corresponding one of the HeLa model. Several variables important for the interpretation of FemX model overlaps with the variables in HeLa model (see below).

In the FemX model, several variables exist that have the same impact (positive or negative), similar weight, and are associated with the same structural fragments of the equivalent compounds as in the HeLa model. These are: TIP–TIP 422, DRY–O 539, O–N1 880, O–TIP 977 and N1–TIP 1125. Brief description of the variables with the highest impact on FemX model is shown in Table 5. On the Fig. 4

Table 3
GRIND variables with the highest impact (positive + or negative −) on the final PLS model, and structural elements of **1**–**33** associated with this variables.

Probe block	Variable no.	Distance (Å)	Impact	Regions
N1–N1	260	7.04–7.36	+	Acetoxy (OAc) groups on ring C (or B for **21** and **26**) *and* the proximal OAc (or amido oxygen) fragment. Did not express only for **1**–**4**
TIP–TIP	422	20.80–21.12	+	*N*-methyl group on ring D or OAc methyl group, *and* the distal alkyl side chain. Present for all compounds, except **1**–**5**
TIP–TIP	471	36.48–36.80	–	Between the two amido *n*-propyl groups on molecules **17** and **20**
DRY–O	539	20.16–20.48	+	Primary or secondary amido NH (O node) *and* angular methyl group (**19**, **20**, **22**, and **24**–**26**) or cyclohexyl moiety (**7**, **8**, **9**, **28**–**33**)
O–N1	880	15.04–15.36	+	Primary or secondary amido nitrogen, *and* tetraoxane ring (**7**, **8**, **9**, **28**–**33**) or OAc group (**19**, **20**, **22**, **24**–**27**)
N1–TIP	1125	17.28–17.60	+	N1 node near the carbonyl oxygen of OAc fragment *and* TIP near methylene group on C–24 atom or methyl group on the distal OAc. Expressed for all molecules except **1**–**4**
N1–TIP	1178	34.24–34.56	–	Amido oxygen *and* distal alkyl part of the compounds **17**, **18** and **20**

Table 4
Statistics of PLS model for antiproliferative potencies of **1**–**33** toward FemX cells.

LVs	X variable explanation	X accumulation	SDEC	SDEP	r^2	q^2 (LOO)	q^2 (LTO)	q^2 (RG)
1	35.56	35.56	0.33	0.38	0.62	0.48	0.48	0.46
2	23.22	58.79	0.23	0.30	0.81	0.68	0.67	0.66
3	14.28	73.06	0.18	0.26	0.89	0.77	0.77	0.74

Abbreviations: SDEC – Standard Deviation of Error of Calculation, SDEP – Standard Deviation of Error of Prediction. One run of FFD variable selection using the following settings: 4 random groups; 20 SDEP; 20% dummies; and Comb/Var ratio = 2. The same validation method is used to calculate q^2 [q^2 (RG) – random groups, q^2 (LTO) – leave two out; q^2 (LOO) – leave one out].

structural elements of molecules associated with variables having highest impact on the model are shown.

The similar spatial arrangement of HBD and HBA regions of molecules are important for the potency of compounds toward both FemX and HeLa cells, as given by variables 539, 880 and 1125. Compounds having acetoxy group in the proximity (less than ~5 Å) to the unsubstituted amido nitrogen, or the amido carbonyl oxygen, or the oxygen atoms of tetraoxane ring exerts lower potency toward FemX cells, given by variables N1–N1 247 and O–N1 849, Fig. 4a and b.

Comparable PLS coefficients plots of HeLa and FemX models (Figs. 1 and 3) indicate that majority among **1**–**33** have similar order of potencies toward each cell lines. Independent confirmation is obtained by the simple plot of the $p(IC_{50})$s of **1**–**33** toward both studied cell lines (Supplementary material, Fig. S4). Compounds **12**–**16** have slightly higher potency toward HeLa cells, and deviate from regularity observed for the rest of compounds.

Inspecting the PLS coefficient plots, it can be seen that the weight of DRY probe (in cross- and auto-correlograms) variables is lower than for the other variables. Hydrophobic interactions may be very important for the potency, because studied set of molecules possesses a large apolar steroidal core, that can interact with an apolar amino acid residues of the, so far unknown, biological target.

It is well known that GRID DRY probe favourably interact with different types of π systems (aromatic or vinyl type), but have not high affinity to aliphatic moieties. Studied compounds, built on steroidal core, or comprising cycloalkyl moiety, lack such π systems. Along with this, GRIND methodology at first extracts local MIF minima of particular probe around molecules; subsequently descriptors were calculated from those points. Consequently, weak non-bonded interactions are encoded in our descriptors, but we try to obtain the independent proof of their importance.

To evaluate whether the hydrophobic properties of the molecules have significant impact on potency, we used GRID to obtain DRY probe MIFs for the whole set of compounds. In the next step, the volumes of the DRY probe interaction regions were extracted from the corresponding MIFs by BIOCUBE. Isocontour level of the DRY probe on −0.3 kcal/mol were chosen as appropriate, because on this level volumes were significantly different from compound to compound (Supplementary material, Fig. S5).

Significant correlation between DRY volumes and $p(IC_{50})$s, for both HeLa and FemX cell lines, was obtained only for the bis-tetraoxane derivatives **17**–**27** (Fig. S6a and b in Supplementary material). Correlation is negative, which implies that the more hydrophobic molecules exert lower potency. Compound **17** is an outlier. This compound has two *N*,*N*-di-*n*-propyl amido groups, which extremely increase the hydrophobicity and the conformational mobility of the whole molecule (virtual log $P = 13.12$ compared to, for example, 6.10 for **19**, Supplementary material, Table S3). So, we can suppose that **17** has a different mechanism of transport into the cell comparing to the other compounds within studied subset. Along with this, in FemX model compound **25** also shows some deviation from correlation.

Although both models (FemX and HeLa) recognized HBD and HBA interactions as highly relevant ones (high intensity of variables in blocks of N1 and O probes), attempts to obtain similar correlation using N1 and O probe isovolumes did not produce significant correlation. Exception was the N1 probe isovolume at −4.0 kcal/mol, versus potency toward FemX cells, for the same subset of compounds (**17**–**27**); Fig. S6c in Supplementary material.

The *n*-octanol–water partition coefficient, expressed as log *P*, is widely applied in the majority of the QSAR models. It is directly related to passive transport through cell membranes, binding to proteins, or binding to active sites of tentative target enzymes. Modest negative linear correlation between the potency toward HeLa and FemX cells and virtual log *P*, are obtained for the whole set of molecules (**1**–**33**), excluding the smallest ones (**1**–**5**), as well as **17** and **25** for the HeLa (Fig. S7a in Supplementary material); and **1**–**5** and **12**–**17** for the FemX model (Fig. S7b in Supplementary material). This is in accordance with observation given in Fig. S6a and b.

Table 5
GRIND variables with highest impact (positive + or negative −) on final PLS model and structural elements of **1**–**33** associated with these variables.

Probe block	Variable no.	Distance (Å)	Impact	Regions
N1–N1	247	2.88–3.20	–	Two closely positioned HBA groups. Present for all compounds, except **3**–**5**
N1–N1	260	7.04–7.36	+	Acetoxy (OAc) groups *and* the carbonyl oxygen of the ring D of the steroid core. Present for all compounds, except **3**–**5**
DRY–O	539	20.16–20.48	+	Primary or secondary amide NH (O node) *and* angular methyl group (for **19**, **20**, **22**, and **24**–**26**) or cyclohexyl moiety (for **7**, **8**, **9**, **28**–**33**)
O–N1	849	5.12–5.44	–	Primary or secondary amido NH *and* proximal OAc group (N1 node). Present for molecules **2**–**5**, **19**–**22**, and **24**–**26**
O–N1	880	15.04–15.36	+	O node proximal to primary or secondary amido NH, *and* N1 node associated to tetraoxane ring (**7**, **8**, **9**, **28**–**33**) or OAc group (**19**–**22**, **24**–**26**)
O–TIP	977	8.00–8.32	–	The O probe node is associated with amido nitrogen; the TIP node is located on *N*-alkyl substituent or on the methyl part of proximal acetoxy moiety
O–TIP	1016	20.48–20.80	+	O nodes are positioned near primary or secondary amide *and* TIP node is near distal alkyl group (4″-Et, OAc, amido alkyl substituents). Expressed for the most potent compounds (**7**–**9**, **19**–**22**, **24**–**26**, **28**–**33**)
N1–TIP	1125	17.28–17.60	+	N1 node is mainly near OAc fragments *and* TIP node is near methylene groups connected to C24 atom, or near to distal OAc fragment. Present for all compounds except **1**–**4**

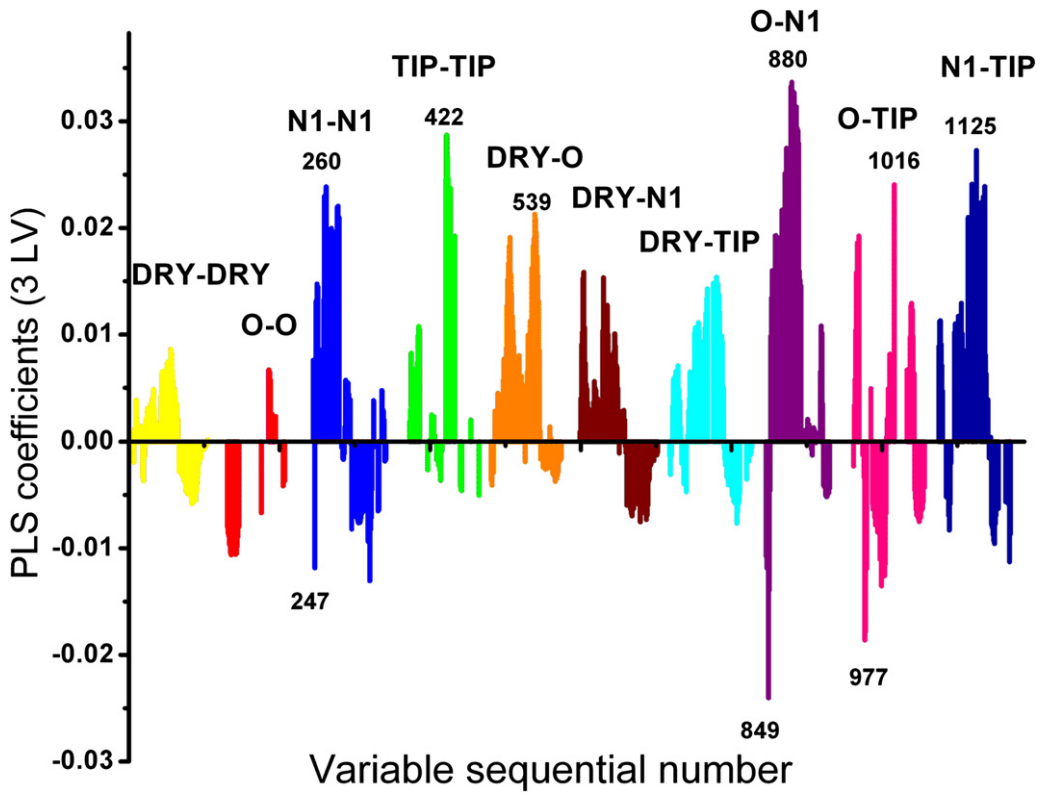

Fig. 3. 3LV PLS coefficients plot for the model on antiproliferative potencies of **1**–**33** toward FemX cells. Graph shows all the auto- and cross-correlograms. The most significant variables are labeled by sequential numbers.

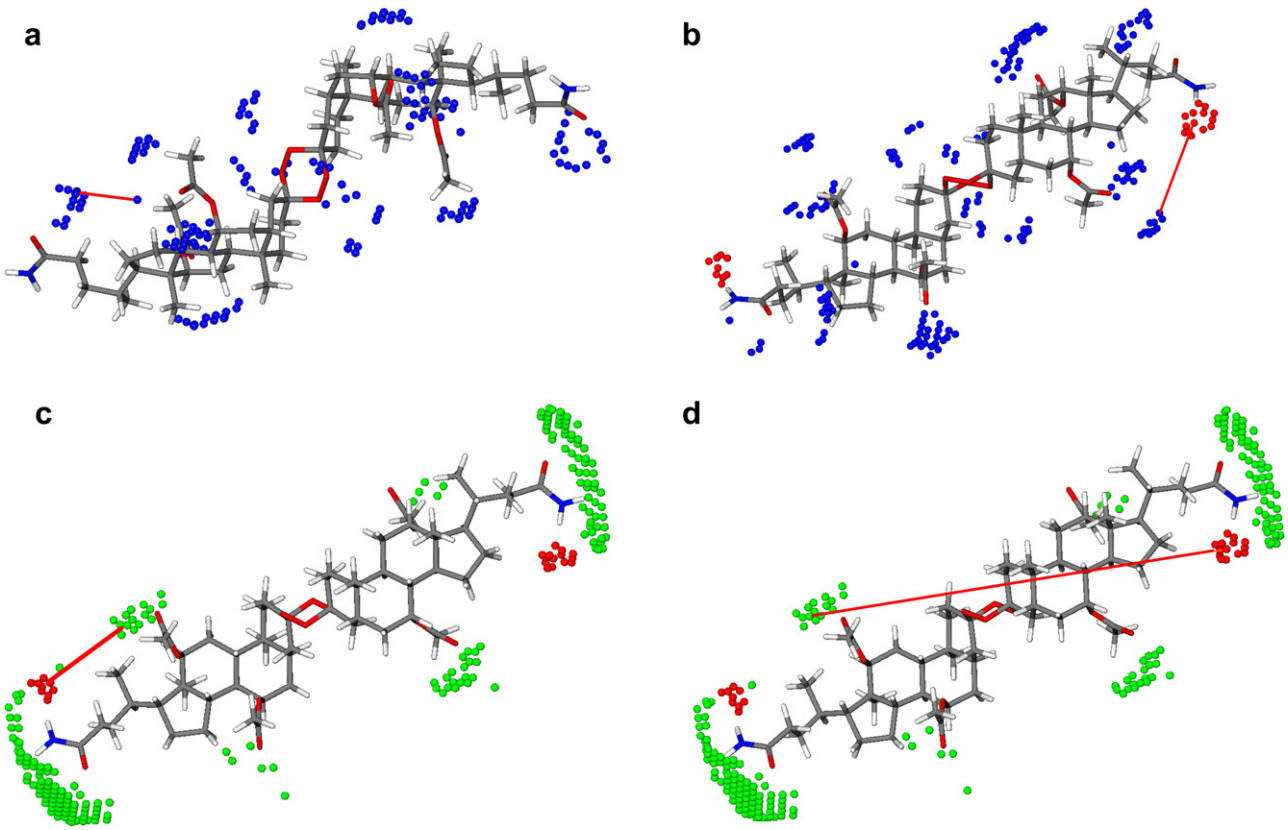

Fig. 4. Association of structural fragments with variables: (a) 247 (N1–N1); (b) 849 (O–N1); (c) 977 (O–TIP); (d) Variable 1016 (O–TIP), for compound **19**.

Attempts to obtain statistically significant multiple linear regression (MLR) model, by using the 3D dependent descriptors (Supplementary material, Table S3), found as relevant the following correlation:

$$\log(1/IC_{50}) = -23.38\ (\pm 6.53) \cdot \text{virt log } P + 0.40\ (\pm 0.31) \cdot \text{O probe isovolume} + 6.15\ (\pm 0.38)\ (n = 26,\ r = 0.87,\ sd = 0.20,\ F = 35.33,\ q^2 = 0.63) \quad (1)$$

Compounds **1**–**5**, **23** and **25** were excluded from the model, as outliers. Probably that **1**–**5** deviate from the correlation because of their small size, and consequently virtual log *P* values incomparable with the rest of compounds; while **23** and **25** are extended by bulky hydrophobic groups on amido moiety.

Virtual log *P* and O probe isovolume, that appear in equation, exert low cross-correlation according to intercorrelation matrix (Supplementary material, Table S4). Three-dimensional plot of virtual log *P*, O probe isovolume and potency of **1**–**33** toward HeLa cells, given in Supplementary material, Fig. S8, shows that more potent compounds are grouped on the higher values of O isovolume and lower virtual log *P*. Therefore, hydrophobicity and H-bond donor ability of **1**–**33** are the main factors that govern potency toward HeLa cells.

Attempts to obtain statistically valid correlations for FemX potency data, by using the same descriptors, failed (all correlations have *r* less then 0.8, and q^2 less then 0.3). Despite of this, in correlations in which virtual log *P* and O isovolumes figured, those descriptors has the same signs as for HeLa model.

Usually, the more hydrophobic compounds exert higher potency because they could pass more efficiently through the phospholipid bilayer of the cell membrane, providing that the passive transport is involved. Negative correlation between potency and virtual log *P* may suggest that majority of studied compounds obey alternative mechanism of transport through the membrane.

Majority of **1**–**33** are cholic acid derivatives (Fig. S8 in Supplementary material). It is known that various Na^+-dependent transporters [17,18] are responsible for the uptake of the bile acids (Na^+/taurocholate cotransporting polypeptide (Ntcp1), organic anion transporting polypeptide (Oatp1), microsomal epoxide hydrolase (mEH)) [19,20], and they can carry some of the functionalized cholic acid derivatives into the cell [21].

Although there is no data that similar transporters exist in HeLa and FemX cells, active transport of studied compounds into the cells might be involved.

3. Conclusion

Molecules having the primary amide group in position 24 of the cholic acid are more potent than secondary and tertiary amides. Steric hindrance that attenuates the H-bond donor ability of amido NH (indicated by the decreased IE with the O probe), or absence of HBDs, has significant negative impact on potency. Consequently, derivatives bearing secondary and tertiary amide groups have attenuated ability to act as HBD and are less potent. Along with this, acetoxy fragments at positions 7 and 12 of steroid core are important for potency of compounds, as can be seen from N1–N1, O–N1 and TIP–TIP variables.

The multivariate linear regressions, independent of derived 3D QSAR models, lead to the same conclusions: the HBD interactions (associated with the O probe) and hydrophobicity (expressed as the virtual log *P*), are the main factors that determine potency toward HeLa and FemX cells, within studied set. The models obtained will be used as guidance for design of novel congeners.

Acknowledgement

Ministry of Science and Technological Development of Serbia support this work, Grant 142010, and 142022.

Appendix. Supplementary data

Supplementary data associated with this article can be found in the online version, at doi:10.1016/j.ejmech.2010.07.019.

References

[1] X.-D. Luo, C.-C. Shen, The chemistry, pharmacology, and clinical applications of Qinghaosu (artemisinin) and its derivatives, Med. Res. Rev. 7 (1987) 29–52.
[2] D.M. Opsenica, B.A. Šolaja, Antimalarial peroxides, J. Serb. Chem. Soc. 74 (2009) 1155–1193 and references cited therein.
[3] J.L. Vennerstrom, H.-N. Fu, W.Y. Ellis, A.L. Ager Jr., J.K. Wood, S.L. Andersen, L. Gerena, W.K. Milhous, Dispiro-1,2,4,5-tetraoxanes: a new class of antimalarial peroxides, J. Med. Chem. 35 (1992) 3023–3027.
[4] (a) C.W. Jefford, A. Jaber, J. Boukouvalas, Efficient preparation of 1,2,4,5-tetraoxanes from bis(trimethylsilyl) peroxide and carbonyl compounds, Synthesis (1988) 391–393;
(b) Y. Dong, J.L. Vennerstrom, Dispiro-1,2,4,5-tetraoxanes *via* ozonolysis of cycloalkanone *O*-methyloximes: a comparison with the peroxidation of cycloalkanones in acetonitrile–sulfuric acid media, J. Org. Chem. 63 (1998) 8582–8585;
(c) Y. Dong, H. Matile, J. Chollet, R. Kaminsky, J.K. Wood, J.L. Vennerstrom, Synthesis and antimalarial activity of 11 dispiro-1,2,4,5-tetraoxane analogues of WR 148999. 7,8,15,16-Tetraoxadispiro[5.2.5.2]hexadecanes substituted at the 1 and 10 positions with unsaturated and polar functional groups, J. Med. Chem. 42 (1999) 1477–1480;
(d) H.-S. Kim, Y. Shibata, Y. Wataya, K. Tsuchiya, A. Masuyama, M. Nojima, Synthesis and antimalarial activity of cyclic peroxides, 1,2,4,5,7-pentoxocanes and 1,2,4,5-tetroxanes, J. Med. Chem. 42 (1999) 2604–2609;
(e) P.H. Dussault, J.M. Raible, Ozonolysis in the presence of Lewis acids: directed addition to carbonyl oxides, Org. Lett. 2 (2000) 3377–3379.
[5] K. Žmitek, S. Stavber, M. Zupan, D. Bonnet-Delpon, J. Iskra, Fluorinated alcohol directed formation of dispiro-1,2,4,5-tetraoxanes by hydrogen peroxide under acid conditions, Tetrahedron 62 (2006) 1479–1484.
[6] Y. Dong, Synthesis and antimalarial activity of 1,2,4,5-tetraoxanes, Mini Rev. Med. Chem. 2 (2002) 113–123.
[7] D. Opsenica, G. Pocsfalvi, Z. Juranić, B. Tinant, J.-P. Declercq, D.E. Kyle, W.K. Milhous, B.A. Šolaja, Cholic acid derivatives as 1,2,4,5-tetraoxane carriers: structure, antimalarial and antiproliferative activity, J. Med. Chem. 43 (2000) 3274–3282.
[8] D. Opsenica, G. Angelovski, G. Pocsfalvi, Z. Juranić, Ž. Žižak, D. Kyle, W.K. Milhous, B.A. Šolaja, Antimalarial and antiproliferative evaluation of bis-steroidal tetraoxanes, Bioorg. Med. Chem. 11 (2003) 2761–2768.
[9] B.A. Šolaja, N. Terzić, G. Pocsfalvi, L. Gerena, B. Tinant, D. Opsenica, W.K. Milhous, Mixed steroidal 1,2,4,5-tetraoxanes: antimalarial and antimycobacterial activity, J. Med. Chem. 45 (2002) 3331–3336.
[10] I. Opsenica, N. Terzić, D. Opsenica, G. Angelovski, M. Lehnig, P. Eilbracht, B. Tinant, Z. Juranić, K.S. Smith, Y.S. Yang, D.S. Diaz, P.L. Smith, W.K. Milhous, D. Đoković, B.A. Šolaja, Tetraoxane antimalarials and their reaction with Fe(II), J. Med. Chem. 49 (2006) 3790–3799.
[11] I. Opsenica, D. Opsenica, K.S. Smith, W.K. Milhous, B.A. Šolaja, Chemical stability of the peroxide bond enables diversified synthesis of potent tetraoxane antimalarials, J. Med. Chem. 51 (2008) 2261–2266.
[12] N. Terzić, D. Opsenica, D. Milić, B. Tinant, K.S. Smith, W.K. Milhous, B.A. Šolaja, Deoxycholic acid derived tetraoxane antimalarials and antiproliferatives, J. Med. Chem. (2007) 5118–5127.
[13] I. Opsenica, N. Terzić, D. Opsenica, W.K. Milhous, B.A. Šolaja, 7,8,15,16-Tetraoxa-dispiro[5.2.5.2]hexadecane-3-carboxylic acid derivatives and their antimalarial activity, J. Serb. Chem. Soc. 69 (2004) 919–922.
[14] Ž. Žižak, Z. Juranić, D. Opsenica, B.A. Šolaja, Mixed steroidal tetraoxanes induce apoptotic cell death in tumor cells, Invest. New Drugs 27 (2009) 432–439.
[15] M. Pastor, G. Cruciani, I. McLay, S. Picket, S. Clementi, GRid-INdependent Descriptors (GRIND): a novel class of alignment-independent three-dimensional molecular descriptors, J. Med. Chem. 43 (2000) 3233–3243.
[16] Á Durán, G.C. Martínez, M. Pastor, Development and validation of AMANDA, a new algorithm for selecting highly relevant regions in molecular interaction fields, J. Chem. Inf. Model. 48 (2008) 1813–1823.
[17] M. Saxena, G.B. Henderson, ATP-dependent efflux of 2,4-dinitrophenyl-*S*-glutathione. Properties of two distinct transport systems in inside-out vesicles from L1210 cells and a variant subline with altered efflux of methotrexate and cholate, J. Biol. Chem. 270 (1995) 5312–5319.

[18] G.B. Henderson, T.R. Hughes, M. Saxena, Functional implications from the effects of 1-chloro-2,4-dinitrobenzene and ethacrynic acid on efflux routes for methotrexate and cholate in L1210 cells, J. Biol. Chem. 269 (1994) 13382–13389.
[19] A.W. Wolkoff, D.E. Cohen, Bile acid regulation of hepatic physiology. I. Hepatocyte transport of bile acids, Am. J. Physiol. Gastrointest. Liver Physiol. 284 (2003) G175–G179.
[20] B. Hagenbuch, Molecular properties of hepatic uptake systems for bile acids and organic anions, J. Membr. Biol. 160 (1997) 1–8.
[21] M. Kågedahl, P.W. Swaan, C.T. Redemann, M. Tang, C.S. Craik, F.C. Szoka Jr., S. Oie, Use of the intestinal bile acid transporter for the uptake of cholic acid conjugates with HIV-1 protease inhibitory activity, Pharm. Res. 14 (1997) 176–180.